

CONVERGENCE OF THE SEMI-DISCRETE WAVEHOLTZ ITERATION*

AMIT ROTEM[†], OLOF RUNBORG[‡], AND DANIEL APPELÖ[†]

Abstract. In this paper we prove that for stable semi-discretizations of the wave equation for the WaveHoltz iteration is guaranteed to converge to an approximate solution of the corresponding frequency domain problem, if it exists. We show that for certain classes of frequency domain problems, the WaveHoltz iteration without acceleration converges in $O(\omega)$ iterations with the constant factor depending logarithmically on the desired tolerance. We conjecture that the Helmholtz problem in open domains with no trapping waves is one such class of problems and we provide numerical examples in one and two dimensions using finite differences and discontinuous Galerkin discretizations which demonstrate these converge results.

Key words. WaveHoltz, Helmholtz, Wave Equation

MSC codes. 65N12, 65N22

1. Introduction. The wave equation is a fundamental mathematical model for describing the propagation of information in physical phenomena such as acoustics, electromagnetism, optics, and fluid dynamics. Its numerical simulations is extensively used to advance research and develop new tools in, for example, communication, imaging, seismic modeling, and engineering.

When simulating the wave equation in the frequency domain we encounter the Helmholtz equation:

$$(1.1) \quad \nabla \cdot (c^2(x)\nabla\hat{u}) + \omega^2\hat{u} = f(x),$$

complemented with suitable boundary conditions. A typical algorithm for approximating solutions to (1.1) discretizes it using finite differences or finite elements, resulting in a linear system of equations

$$(L - \omega^2 M)\hat{u}_h = -f_h,$$

for the representation of the approximate solution \hat{u}_h . Here L approximates the negative Laplacian ($L\hat{u}_h \approx -\nabla \cdot (c^2\nabla\hat{u})$) and M is either a mass matrix in the finite element context or the identity in the finite difference context. To this end, the subscript h identifies the quantities that are approximations (here, by a finite difference or discontinuous Galerkin method). For energy conserving boundary conditions (Dirichlet or Neumann), the matrix L is often symmetric and positive semi-definite, similarly M is necessarily symmetric positive definite, therefore the matrix $L - \omega^2 M$ is usually indefinite. For boundary conditions which dissipate energy, L may be complex symmetric (not Hermitian) or not symmetric at all.

When ω is large, the solution is highly oscillatory and it needs to be resolved by many degrees of freedom. For a finite difference or finite element method of order p , to sufficiently resolve the solution we require

$$\omega^{p+1}h^p = \text{const.} \implies \#\text{DOFs} \sim O(\omega^{1+1/p}).$$

*Submitted to the editors.

Funding: This work was supported by the National Science Foundation Grant NSF DMS-2208164. Any opinions, findings, and conclusions or recommendations expressed in this material are those of the authors and do not necessarily reflect the views of the National Science Foundation.

[†]Department of Mathematics, Virginia Tech, Blacksburg, VA (arotem@vt.edu).

[‡]Department of Mathematics, Royal Institute of Technology, Stockholm, Sweden.

Here h is the scale of the mesh [9]. For high frequency problems, the number of degrees of freedom can easily exceed tens of thousands in two dimensions, and millions in three dimensions.

The indefinite nature of the Helmholtz equation makes it challenging for classical iterative algorithms. Highly efficient iterative methods for the similar (yet definite) Poisson equation,

$$-\nabla \cdot (c^2(x)\nabla \hat{u}) = f,$$

often fail for the Helmholtz equation. For example, since the Helmholtz equation is indefinite the popular conjugate gradient method is inapplicable and other methods such as GMRES or the biconjugate method must be used instead. Yet still, these methods converge much more slowly for the indefinite problem than for the definite one. Other iterative methods, developed for Poisson's equation, such as Schwartz domain decomposition or multigrid, entirely fail to converge for the Helmholtz equation and fail to substantially improve convergence as preconditioners for GMRES [10, 9].

To remedy this difficulty, specialized algorithms for the Helmholtz equation have been introduced. For example, the domain decomposition method of Després which replaces the Dirichlet condition of the classical Schwartz iteration with impedance conditions [7], or the wave-ray multigrid method of Brandt and Livshits in which the typical smoothing step is replaced by ray-cycles [4] (see also [10, 9]). Additionally, there have been extensive developments of preconditioning techniques such as ILU factorizations, or methods which solve the complex-shifted Laplacian as a means to control the distribution of the eigenvalues of the preconditioned system. The sweeping preconditioner of Engquist and Ying (see [8]) which uses the approximate low rank structure of the Green's function to construct an approximate LU factorization that can be computed and applied efficiently and substantially reduces the number of iterations of GMRES.

There are also several direct methods for solving Helmholtz equation, for example the Hierarchically Semi-Separable (HSS) parallel multifrontal sparse solver by deHoop and co-authors, [22], and the spectral collocation solver by Gillman, Barnett and Martinsson, [12]. Of course, integral equations have a long history and a complete literature review is beyond the scope of this introduction and we refer the reader to the review [19] and its 400+ references.

An entirely different set of algorithms solve the Helmholtz equation by solving a closely related wave equation in the time domain. Controllability methods, for example, solve the Helmholtz equation by minimizing the difference between the initial condition and the solution of the wave equation after one period ($2\pi/\omega$) in time. The solution to the Helmholtz equation is the initial condition that minimizes this difference, and the minimization problem can be solved with the conjugate gradient method. The original controllability method can be found in [5] and more recent developments and extensions can be found in [15, 13, 16].

Another iterative method, and the focus of this paper, is the WaveHoltz algorithm which solves the Helmholtz equation by repeatedly filtering the solution to the wave equation in the time domain. The resulting fixed point iteration can be accelerated by Krylov methods, and, in contrast to classical discretizations, the system of equations from WaveHoltz is positive definite for energy conserving boundary conditions. When energy is not necessarily conserved, the WaveHoltz iteration still benefits from the efficiency of high performance wave equation solvers.

In the first half of this paper we present a new result which guarantees convergence of the WaveHoltz iteration itself, for any stable semi-discretization of the wave

equation, to the approximate solution of the Helmholtz equation, provided it exists. More precisely, this result requires that the eigenvalues of the discretization matrix have non-positive real parts and are not equal to $\pm i\omega$, with the convergence rate improving as the smallest distance $\pm i\omega$ to increases. Further, for certain classes of problems, we demonstrate that the convergence rate of the fixed point iteration is $O(1 - \omega^{-1})$; our numerical experiments suggest that problems in open domains which do not trap waves satisfy these conditions. After presenting these theoretical results, we will consider a few numerical examples in which these results are realized. First we will investigate one dimensional problems with impedance boundary conditions. We will investigate the distribution of eigenvalues of the discretization matrix and find that, indeed, the eigenvalues of these matrices appear uniformly bounded away from $\pm i\omega$. Afterwards, we will investigate the convergence rates for similar problems in two dimensions. We then observe that more iterations are needed to converge but the $O(1 - \omega^{-1})$ convergence rate is preserved. For results relating to closed domains (energy conserving boundary conditions) we refer the reader to the original paper, [3].

The paper is organized as follows. In Section 2 we will summarize the WaveHoltz algorithm and previous convergence results. We will also define the semi-discrete WaveHoltz iteration and show that the solution to the discretized Helmholtz equation is a fixed point of the iteration. In Section 3 we prove the convergence result for the semi-discrete WaveHoltz iteration. Lastly, in Section 4 we perform numerical experiments which relate the theoretical results to two common discretizations of the wave equation.

2. The WaveHoltz Iteration. In this paper, our goal is to solve the Helmholtz equation

$$(2.1a) \quad \nabla \cdot (c^2(x)\nabla \hat{u}) + \omega^2 \hat{u} = f(x), \quad x \in \Omega,$$

$$(2.1b) \quad i\omega\alpha \hat{u} + \beta(\mathbf{n} \cdot c^2(x)\nabla \hat{u}) = 0, \quad x \in \partial\Omega.$$

Here Ω is an open and simply connected subset of \mathbb{R}^d ($d = 1, 2, 3$) with boundary $\partial\Omega$, and $\alpha^2 + \beta^2 = 1$ with α and β possibly varying in $\partial\Omega$. Consider the function $u(x, t) = \hat{u}(x)e^{i\omega t}$. If we differentiate u twice in time we find:

$$u_{tt} = -\omega^2 \hat{u} e^{i\omega t} = [\nabla \cdot (c^2(x)\nabla \hat{u}) - f(x)] e^{i\omega t}.$$

That is, u satisfies the wave equation:

$$(2.2a) \quad u_{tt} = \nabla \cdot (c^2(x)\nabla u) - f(x)e^{i\omega t}, \quad x \in \Omega, t > 0$$

$$(2.2b) \quad \alpha u_t + \beta(\mathbf{n} \cdot c^2(x)\nabla u) = 0, \quad x \in \partial\Omega, t > 0.$$

The wave equation is an easier equation to solve because fast, memory lean, and robust numerical methods for the wave equation are readily available. The aim of the WaveHoltz algorithm is to use the efficiency of wave equation solvers to solve the Helmholtz equation.

In Section 2.1, we will introduce the WaveHoltz algorithm as a theoretical framework applied to exact solutions of the wave equation and discuss how the wave equation is used to solve the Helmholtz equation. Further, we will summarize previous notable results about the WaveHoltz algorithm. In Section 2.2, we will introduce the iteration as it is applied in a “semi-discrete” setting, where we have discretized in space but remain continuous in time. We will reformulate the WaveHoltz iteration and apply it to the semi-discrete wave equation which we will write as a *first order* system in time. Such a formulation is very general because the wave equation

naturally appears as a first order system in the context of hyperbolic conservation laws, while second order equations are easily converted to first order by introducing a “velocity” variable.

2.1. Exact Iteration. Consider Helmholtz equation (2.1). The WaveHoltz iterative algorithm [3] approximates the solution to Helmholtz equation by filtering solutions of the time dependent wave equation in the fixed point iteration,

$$\begin{pmatrix} \hat{u}^{(n+1)} \\ \hat{v}^{(n+1)} \end{pmatrix} = \Pi \begin{pmatrix} \hat{u}^{(n)} \\ \hat{v}^{(n)} \end{pmatrix},$$

where $\hat{u} = \hat{u}(x)$, $\hat{v} = \hat{v}(x)$, and Π is defined as

$$(2.3) \quad \Pi \begin{pmatrix} \hat{u} \\ \hat{v} \end{pmatrix} = \frac{2}{T} \int_0^T \left(\cos(\omega t) - \frac{1}{4} \right) \begin{pmatrix} u \\ u_t \end{pmatrix} dt, \quad T = \frac{2\pi}{\omega},$$

and $u = u(x, t)$ solves wave equation (2.2) with initial conditions

$$u(x, 0) = \hat{u}(x), \quad u_t(x, 0) = \hat{v}(x).$$

Intuitively, the integration kernel is designed to damp all time harmonic modes of the solution with frequency not equal to ω , while preserving the ω frequency mode. If the initial conditions to the wave equation are $u(x, 0) = \hat{u}(x)$ and $u_t(x, 0) = i\omega\hat{u}(x)$, then the solution is $u(x, t) = \hat{u}(x)e^{i\omega t}$. Hence, because

$$(2.4) \quad \frac{2}{T} \int_0^T \left(\cos(\omega t) - \frac{1}{4} \right) e^{i\omega t} dt = 1,$$

the integral in (2.3) evaluates to $[\hat{u}(x), i\omega\hat{u}(x)]^T$. Thus, by construction, the solution \hat{u} to the Helmholtz equation corresponds to the fixed-point

$$\begin{pmatrix} \hat{u} \\ i\omega\hat{u} \end{pmatrix} = \Pi \begin{pmatrix} \hat{u} \\ i\omega\hat{u} \end{pmatrix}.$$

For energy conserving boundary conditions ($\alpha = 0$ or $\beta = 0$ in (2.1b)), the operator Π is contractive as long as ω^2 is not an eigenvalue of $-\nabla \cdot (c^2 \nabla)$ (i.e. if ω is not a resonant frequency) so the iteration converges to the fixed-point $(\hat{u}, i\omega\hat{u})$ for any initial condition $(\hat{u}^{(0)}, \hat{v}^{(0)})$. Additionally, the operator Π is affine, so $\Pi \begin{pmatrix} \hat{u} \\ \hat{v} \end{pmatrix}$ can be decomposed as the action of a linear operator \mathcal{S} plus a function π_0 which does not depend on (\hat{u}, \hat{v}) , that is,

$$\Pi \begin{pmatrix} \hat{u} \\ \hat{v} \end{pmatrix} = \mathcal{S} \begin{pmatrix} \hat{u} \\ \hat{v} \end{pmatrix} + \pi_0, \quad \pi_0 = \Pi \begin{pmatrix} 0 \\ 0 \end{pmatrix},$$

where

$$\begin{aligned} \mathcal{S} \begin{pmatrix} \hat{u} \\ \hat{v} \end{pmatrix} &= \frac{2}{T} \int_0^T \left(\cos(\omega t) - \frac{1}{4} \right) \begin{pmatrix} u \\ u_t \end{pmatrix} dt, \\ \frac{\partial^2 u}{\partial t^2} &= \nabla \cdot (c^2(x) \nabla u), \quad u(x, 0) = \hat{u}(x), \quad u_t(x, 0) = \hat{v}(x). \end{aligned}$$

Note that the wave equation here is homogeneous. Moreover, the fixed point equation is equivalent to the linear operator equation

$$(\mathcal{I} - \mathcal{S}) \begin{pmatrix} \hat{u} \\ \hat{v} \end{pmatrix} = \pi_0.$$

Hence, once discretized the fixed-point iteration can be accelerated by Krylov space methods such as GMRES where the action of the discretized operator \mathcal{S} is computed by numerically solving the wave equation and approximating the filter by quadrature.

For energy conserving boundary conditions \hat{v} is not needed and the iteration can be further simplified to $\hat{u}^{(n+1)} = \Pi \hat{u}^{(n)}$. Here Π is defined as before but always taking $\hat{v}^{(n)} = u_t(x, 0) = 0$. In this regime, the convergence rate was estimated to be [3]

$$\frac{\|\hat{u}^{(n+1)} - \hat{u}\|}{\|\hat{u}^{(n)} - \hat{u}\|} \sim 1 - \frac{1}{\omega^{2d}}.$$

Thus the number of iterations to reach some specified tolerance is $O(\omega^{2d})$ where d is the spatial dimension. However, for energy conserving boundary conditions, the operator $\mathcal{I} - \mathcal{S}$ is positive and self adjoint. Thus (after discretization) the linear system can be solved with the conjugate gradient method in $\mathcal{O}(\omega^d)$ iterations (see [3]). This is a notable advantage of the WaveHoltz algorithm because direct discretizations of the Helmholtz equation do not lead to definite systems and thus cannot be solved with the conjugate gradient method. These results for the energy conserving case for the continuous and time discrete problem were proved in [3], but the properties of the WaveHoltz algorithm in the spatially discrete setting have not yet been considered. In this paper we generalize these results in the discrete setting to apply to any stable discretizations which therefore applies to any boundary conditions which conserve or dissipate energy.

2.2. Semi-Discrete Iteration. In each step of the WaveHoltz iteration we solve the wave equation in (2.2). We begin by rewriting this equation as a first order system in time. We consider two possible representations. First, we introduce the velocity variable v and write

$$(2.5a) \quad u_t = v,$$

$$(2.5b) \quad v_t = \nabla \cdot (c^2 \nabla u) - f(x)e^{i\omega t}.$$

Second, we write the wave equation as the linear first order hyperbolic system:

$$(2.6a) \quad p_t + \nabla \cdot (c^2 \mathbf{u}) = -\frac{1}{i\omega} f(x)e^{i\omega t},$$

$$(2.6b) \quad \mathbf{u}_t + \nabla p = 0.$$

Observe that differentiating (2.6a) in time, switching the order of differentiation, and substituting (2.6b) we recover

$$p_{tt} = \nabla \cdot (c^2 \nabla p) - f(x)e^{i\omega t},$$

which is our original wave equation. Similar arguments can be made for other first order systems (e.g. Maxwell's equations is a notable application, see [20]), but we will focus on these two systems as representative examples.

In Section 4.1.1, we will approximate the system, (2.5), with a finite difference method, and in Section 4.1.2 we will approximate the system, (2.6), using a Discontinuous Galerkin method. In both cases and once the equations have been discretized in space they can be written as a first order system of ordinary differential equations.

For example, let $w_h \in \mathbb{C}^m$ be the spatial degrees of freedom which collectively represents approximations to both u and v in system (2.5) or p and \mathbf{u} in system (2.6). The semi-discretization of the wave equation (on either form) can then be written

$$(2.7) \quad \frac{dw_h}{dt} = Aw_h - Fe^{i\omega t}.$$

Here $A \in \mathbb{R}^{m \times m}$ is an approximation of the spatial operators and $F \in \mathbb{R}^m$ contains an approximation of the forcing $f(x)$. For example, we may discretize system (2.5) as $w_h = (u_h, v_h)^T$ and

$$A = \begin{pmatrix} 0 & I \\ -L & B \end{pmatrix}, \quad F = \begin{pmatrix} f_h \\ 0 \end{pmatrix}.$$

Here I is the identity matrix, L approximates $-\nabla \cdot (c^2 \nabla)$ and B approximates boundary conditions (see Section 4.1.1). From this system, the spatial discretization of the WaveHoltz operator Π_h and associated iteration are

$$(2.8) \quad \hat{w}_h^{(n+1)} = \Pi_h \hat{w}_h^{(n)}, \quad \Pi_h \hat{w}_h = \frac{2}{T} \int_0^T \left(\cos(\omega t) - \frac{1}{4} \right) w_h(t) dt,$$

$$\frac{dw_h}{dt} = Aw_h - Fe^{i\omega t}, \quad w_h(0) = \hat{w}_h.$$

As in the fully continuous case we also define the corresponding discretized operators \mathcal{S}_h and $\pi_{0,h}$ satisfying $\Pi_h \hat{w}_h = \mathcal{S}_h \hat{w}_h + \pi_{0,h}$. Let \hat{w}_h^* solve

$$(2.9) \quad i\omega \hat{w}_h^* = A\hat{w}_h^* - F.$$

Then $\hat{w}_h^* e^{i\omega t}$ solves (2.7) with initial condition $w_h(0) = \hat{w}_h^*$, and by (2.4) it is a fixed point of Π_h ,

$$\hat{w}_h^* = \Pi_h \hat{w}_h^*.$$

In the context of system (2.5), we have $\hat{w}_h^* = (\hat{u}_h^*, \hat{v}_h^*)^T$ and we can eliminate \hat{v}_h^* to find that \hat{u}_h^* solves the system

$$(2.10) \quad \tilde{L} \hat{u}_h^* - \omega^2 \hat{u}_h^* = -f_h, \quad \tilde{L} = L - \frac{1}{i\omega} B,$$

which is the discretized Helmholtz equation. Because of this equivalency we refer to (2.9) as the discrete Helmholtz equation. Consequently, the quality of \hat{u}_h^* as an approximation to the solution \hat{u} mainly depends on the quality of the spatial discretization. In practice, the differential equation, (2.7), is discretized in time. The error of the time stepping scheme and quadrature rule in the computation of (2.8) introduces an error, and accordingly the fixed point \hat{w}_h^* is not the exact fixed point of the iteration discretized in time. Nevertheless the error vanishes as $\Delta t \rightarrow 0$. All the same, the error introduced by the time integration can be eliminated by applying a corrected time stepping scheme [21] and tuning the filter to $\cos(\omega t) - a(t)$, see [2].

In the following section we provide sufficient conditions for convergence of the semi-discrete WaveHoltz iteration to the approximate solution of the Helmholtz problem \hat{w}_h^* .

3. Convergence Theory for the Semi-Discrete Iteration. In this section we will analyze the semi-discrete version of the WaveHoltz iteration for approximating solutions to the Helmholtz equations and discuss sufficient conditions for convergence for a stable discretization. We let \hat{w}_h^* be the solution to the discrete Helmholtz equation (2.9). Then as we showed above, it is also a fixed point of (2.8). The main result establishing convergence is the following theorem.

THEOREM 3.1. *Denote by $\|\cdot\|$ any p -norm on \mathbb{C}^m , and when its argument is a matrix, let $\|\cdot\|$ denote the corresponding induced norm. Let $\hat{w}_h^* \in \mathbb{C}^m$ be the solution of (2.9) and denote by $\hat{w}_h^{(n)} \in \mathbb{C}^m$ the n^{th} iterate generated by the WaveHoltz iteration (2.8) with initial condition $\hat{w}_h^{(0)}$. Suppose $A \in \mathbb{R}^{m \times m}$ can be diagonalized as $A = R\Lambda R^{-1}$ and all of its eigenvalues $\{\lambda_j\}_{j=1}^m$ have non-positive real part. If there exists an $\varepsilon = \varepsilon(m, \omega) > 0$ such that for all $\lambda_j/\omega = x + iy \in \mathbb{C}_-$,*

$$(3.1) \quad -x + \alpha(y-1)^2 > \varepsilon, \quad \text{and} \quad -x + \alpha(y+1)^2 > \varepsilon,$$

where $\alpha = \frac{2\pi^2-3}{12\pi} \approx 0.44$, then $\hat{w}_h^{(n)} \rightarrow \hat{w}_h^*$ and there is a convergence rate $r \in (0, 1)$ satisfying

$$(3.2) \quad r \leq \max\{1 - \varepsilon, 1 - \delta\},$$

with $\delta \in (0, 1)$ a universal constant, such that

$$(3.3) \quad \|R^{-1}(\hat{w}_h^{(n+1)} - \hat{w}_h^*)\| \leq r \|R^{-1}(\hat{w}_h^{(n)} - \hat{w}_h^*)\|.$$

Moreover, if $\kappa(m)$ is the condition number of $R \in \mathbb{C}^{m \times m}$ then

$$(3.4) \quad \|\hat{w}_h^{(n)} - \hat{w}_h^*\| \leq \kappa(m)r^n \|\hat{w}_h^{(0)} - \hat{w}_h^*\|.$$

To have an accurate solution the system size will grow with ω , that is $m = m(\omega)$. If a bound on the condition number $\kappa(m(\omega)) \leq M\omega^\gamma$ for some $M, \gamma > 0$, can be established, then the minimum number of iterations needed to reach a given tolerance $\tau > 0$ is no greater than

$$(3.5) \quad N(\tau, \omega) := \frac{\gamma \log(M\omega) - \log(\tau)}{\varepsilon}.$$

In other words, for all iterates $n \geq N(\tau, \omega)$

$$(3.6) \quad \|\hat{w}_h^{(n)} - \hat{w}_h^*\| \leq \tau \|\hat{w}_h^{(0)} - \hat{w}_h^*\|.$$

We now make some observations about Theorem 3.1 and its consequences. Note that the precise estimates (3.2) and (3.3) are for the coefficients $R^{-1}\hat{w}_h$ in the expansion in the eigenvectors of A , and the looser bound (3.4) is for the solution itself. Since we do not assume that R is unitary, $\|R^{-1}(\hat{w}_h^{(n+1)} - \hat{w}_h^*)\|$ may be much smaller than the actual error $\|\hat{w}_h^{(n+1)} - \hat{w}_h^*\|$ for some n . This could occur when the eigenvectors of A are nearly linearly dependent.

Further, any non-singular discretization of Helmholtz equation will satisfy the requirement that $\varepsilon > 0$ and the parameter ε is a consequence of the discretization and the physical problem setup rather than something introduced by the WaveHoltz iteration.

As mentioned in the introduction it is customary to choose the discretization size h so that

$$(3.7) \quad \omega^{p+1}h^p = \text{const.}$$

and the assumption that m depends on ω is a consequence of this. We note that, based on our numerical experiments in Section 4, the condition that κ is bounded by a polynomial in ω does not appear to be a restrictive assumption.

So far, we have left the relationship between ε and ω rather abstract. This is because the relationship is highly problem dependant, but we now summarize the convergence results precisely in terms of the relationship between ω and ε in the context of two prototypical physical settings. Let λ^* be the closest eigenvalue to $i\omega$ in the sense of the parabolic distance, that is,

$$(3.8) \quad \lambda^* = \arg \min_{\lambda_j/\omega = x_j + iy_j} -x_j + \alpha(y_j - 1)^2.$$

Write $\lambda^*/\omega = x + iy$, the smallest value of ε we can take in Theorem 3.1 is

$$(3.9) \quad \varepsilon^* = -x + \alpha(y - 1)^2.$$

We will also consider the Euclidean distance $|\lambda^* - i\omega|$, and assume

$$|\lambda^* - i\omega| \geq C\omega^{-s},$$

for some $C > 0, s \geq 0$ which are problem dependant. This assumption states that as ω and therefore m increases due to (3.7), the eigenvalues of A get denser and therefore the distance $|\lambda^* - i\omega|$ shrinks, but that we can bound the rate at which it shrinks. We characterize the number of iterations to convergence for problems with and without trapped waves for the two prototypical cases below:

- (A) *Problems in open domains with no trapping waves.* For such problems, the physics suggest that all of the energy will eventually be transported out of the domain, and therefore we expect all of the eigenvalues of A to have a strictly negative real part. In particular, we observe empirically that $-x \gg \alpha(y - 1)^2$. Then

$$(3.10) \quad N(\tau, \omega) \leq \frac{\gamma\omega \log(M\omega) - \omega \log(\tau)}{-\Re\{\lambda^*\}} \approx \frac{\gamma\omega \log(M\omega) - \omega \log(\tau)}{|\lambda^* - i\omega|} \\ \sim O(\omega^{1+s} \log \omega + \omega^{1+s} |\log \tau|).$$

Note that only the second of the two terms in (3.10) depends on the tolerance τ . In the one dimensional tests, we observe that the distance from the imaginary axis appears to depend sublinearly on $1/\omega$, so that $s < 1$. Moreover, we do not see the effects of the faster growing $O(\omega^{1+s} \log \omega)$ term. This may indicate that the analysis could be sharpened to remove this term.

- (B) *Problems with energy conserving boundary conditions.* For these problems, we expect all of the eigenvalues of A to be imaginary. More generally, if $-x \ll \alpha(y - 1)^2$, then

$$N(\tau, \omega) \leq \frac{\gamma\omega^2 \log(M\omega) - \omega^2 \log(\tau)}{\alpha \Im\{\lambda^* - i\omega\}^2} \approx \frac{\gamma\omega^2 \log(M\omega) - \omega^2 \log(\tau)}{\alpha |\lambda^* - i\omega|^2} \\ \sim O(\omega^{2+2s} \log \omega + \omega^{2+2s} |\log \tau|).$$

For energy conserving discretizations, the discretization of the Laplacian is typically symmetric, so A is normal with all of its eigenvalues lying on a segment of the imaginary axis and the eigenvalues cover this segment more and more densely as ω (and thus m) increases. If A is normal, then $\kappa(m) \equiv 1$, meaning that $M = 1$ and $\gamma = 0$. The logarithmic term then drops out so we have the estimate

$$N(\tau, \omega) \sim O(\omega^{2+2s} |\log \tau|).$$

The rate at which the eigenvalues cover the line segment increases exponentially with the dimension of the problem. For the problem to be well resolved, $i\omega$ has to fall in the range of these eigenvalues and thus the eigenvalues can fall very closely to $i\omega$. Based on the Weyl asymptotic estimate of the eigenvalues of the continuous Laplacian we expect $|\lambda^* - i\omega| \sim \omega^{1-d}$, that is $s = d - 1$, on average for large ω and λ , which coincides with the estimate $N \sim O(\omega^{2d})$ in [3].

To generalize Theorem 3.1 to the case when A is non-diagonalizable we present the following theorem whose proof is found in Appendix A.

THEOREM 3.2. *Under the same assumptions as in Theorem 3.1 with the exception that A is not necessarily diagonalizable, $\hat{w}_h^{(n)} \rightarrow \hat{w}_h^*$ and there is a convergence rate $r \in (0, 1)$ satisfying*

$$r \leq \max \left\{ 1 - \frac{1}{2}\varepsilon, 1 - \frac{1}{2}\delta \right\},$$

with δ the same as in Theorem 3.1, such that

$$(3.11) \quad \|\hat{w}_h^{(n)} - \hat{w}_h^*\| \leq Kr^n \|\hat{w}_h^{(0)} - \hat{w}_h^*\|.$$

Here $K = K(A, \varepsilon, \|\cdot\|)$ is some constant independent of the iteration number n .

The error bounds in Theorem 3.2 are less precise than in 3.1 as not much can be said about the constant K in general. Nevertheless, the generalization to non-diagonalizable discretizations is important because upwind type discretizations are often not diagonalizable. Consider for example the most basic upwind finite difference discretization of $w_t + w_x = 0$, i.e.

$$\frac{dw_j}{dt} + \frac{w_j - w_{j-1}}{h} = 0.$$

For this discretization the matrix $-hA$ is bi-diagonal with ones on diagonal and negative ones on the first lower diagonal. The eigenvalues of A are all $-h^{-1}$, but A has only the single eigenvector $(0, \dots, 0, 1)^T$ and thus is not diagonalizable. Other upwind discretizations like the discontinuous Galerkin method with upwind flux are also not diagonalizable. In Section 4.3.2 we will see that DG with upwind and central fluxes produce very similar iterations with WaveHoltz. This suggests that a different analysis not based on diagonalization and bounds on the condition number should be possible. Such analysis is left for the future.

3.1. Proof of Theorem 3.1. Before presenting the proof of Theorem 3.1, we introduce the filter-transfer function which is central to this proof.

DEFINITION 3.3 (Filter-Transfer Function).

For a Helmholtz frequency ω , the filter-transfer function β is defined as

$$\beta(\lambda) = \frac{2}{T} \int_0^T \left(\cos(\omega t) - \frac{1}{4} \right) e^{\lambda t} dt, \quad T = \frac{2\pi}{\omega}.$$

We also introduce the scaled filter-transfer function $\hat{\beta}(z)$,

$$\hat{\beta}(z) := \beta(\omega z) = \frac{1}{\pi} \int_0^{2\pi} \left(\cos(s) - \frac{1}{4} \right) e^{zs} ds,$$

which is independent of ω .

We now turn to the main proof. It relies on a number of supporting lemmas proved in the next subsection, which are here tied together into a full proof.

To determine how $\hat{w}_h^{(n)}$ converges to \hat{w}_h^* , we analyze the residual vector at the n -th iteration $\hat{e}_h^{(n)} := \hat{w}_h^{(n)} - \hat{w}_h^*$. Substituting $\hat{w}_h^{(n)} = \hat{w}_h^* + \hat{e}_h^{(n)}$ into (2.8) we find

$$\begin{aligned} \hat{w}_h^* + \hat{e}_h^{(n+1)} &= \Pi_h(\hat{w}_h^* + \hat{e}_h^{(n)}) = \mathcal{S}_h(\hat{w}_h^* + \hat{e}_h^{(n)}) + \pi_{0,h} \\ &= \mathcal{S}_h \hat{w}_h^* + \pi_{0,h} + \mathcal{S}_h \hat{e}_h^{(n)} = \Pi_h \hat{w}_h^* + \mathcal{S}_h \hat{e}_h^{(n)}. \end{aligned}$$

Since \hat{w}_h^* is a fixed point of Π_h , this simplifies to

$$(3.12) \quad \hat{e}_h^{(n+1)} = \mathcal{S}_h \hat{e}_h^{(n)} \implies \hat{e}_h^{(n)} = (\mathcal{S}_h)^n \hat{e}_h^{(0)}.$$

If $\hat{e}_h^{(n)} \rightarrow 0$, then $\hat{w}_h^{(n)} \rightarrow \hat{w}_h^*$, so we must show that \mathcal{S}_h is eventually contractive, that is, there is some power k , such that $\|(\mathcal{S}_h)^k\| < 1$. To this end, it is sufficient to show that $\rho(\mathcal{S}_h) < 1$ which we achieve by relating \mathcal{S}_h to A .

The product $\mathcal{S}_h \hat{e}_h$ is

$$(3.13a) \quad \mathcal{S}_h \hat{e}_h = \frac{2}{T} \int_0^T \left(\cos(\omega t) - \frac{1}{4} \right) e_h(t) dt,$$

$$(3.13b) \quad \frac{de_h}{dt} = A e_h, \quad e_h(0) = \hat{e}_h.$$

By assumption, $A = R\Lambda R^{-1}$, and since we do not assume that A is normal, R is generally not unitary, and its eigenvalues $\lambda_j = \Lambda_{jj}$, $j = 1, \dots, m$ are complex. The solution to (3.13b) is

$$e_h(t) = e^{tA} \hat{e}_h = R e^{t\Lambda} R^{-1} \hat{e}_h.$$

and thus,

$$\mathcal{S}_h \hat{e}_h = R \left(\frac{2}{T} \int_0^T \left(\cos(\omega t) - \frac{1}{4} \right) e^{t\Lambda} dt \right) R^{-1} \hat{e}_h.$$

Since this is true for any \hat{e}_h , we conclude that

$$(3.14) \quad \mathcal{S}_h = R S R^{-1},$$

where S is a diagonal matrix (because $e^{t\Lambda}$ is diagonal) with entries

$$S_{jj} = \frac{2}{T} \int_0^T \left(\cos(\omega t) - \frac{1}{4} \right) e^{\lambda_j t} dt = \beta(\lambda_j), \quad j = 1, \dots, m.$$

Here, we recall that β is the filter transfer function from Definition 3.3. Thus, \mathcal{S}_h has the same eigenvectors as A , and its eigenvalues are the eigenvalues of A mapped by the filter transfer function. Substituting (3.14) into (3.12) we have,

$$\hat{e}_h^{(n+1)} = R S R^{-1} \hat{e}_h^{(n)}, \quad \text{and} \quad \hat{e}_h^{(n)} = R S^n R^{-1} \hat{e}_h^{(0)}.$$

To both equations, we multiply both sides by R^{-1} , take the norm, and using the sub-multiplicative property of the matrix norm to conclude that

$$\|R^{-1}\hat{e}_h^{(n+1)}\| \leq r\|R^{-1}\hat{e}_h^{(0)}\|, \quad \text{and} \quad \|\hat{e}_h^{(n)}\| \leq \kappa(R)r^n \cdot \|\hat{e}_h^{(0)}\|,$$

where, since S is diagonal and $\|\cdot\|$ is a p -norm, $r = \|S\| = \rho(S)$ is the spectral radius of S , and $\kappa(R) = \|R\| \cdot \|R^{-1}\|$ is the condition number of R . Since $\kappa(R)$ is independent of the iteration, we only need $r^n \rightarrow 0$ i.e. $\rho(S) < 1$ to ensure that $\|\hat{e}_h^{(n)}\| \rightarrow 0$. Since we assume that there exists an $\varepsilon > 0$ such that

$$-\Re\{\lambda_j/\omega\} + \alpha(\Im\{\lambda_j/\omega\} - 1)^2 \geq \varepsilon, \quad \text{and} \quad -\Re\{\lambda_j/\omega\} + \alpha(\Im\{\lambda_j/\omega\} + 1)^2 \geq \varepsilon,$$

for each j , then by Lemma 3.8,

$$r \leq \max\{1 - \varepsilon, 1 - \delta\} < 1.$$

This proves (3.3) and (3.4). Next, assume $n \geq N(\tau, \omega)$, then since $\varepsilon \leq -\log(1 - \varepsilon)$

$$n \geq \frac{\gamma \log(M\omega) - \log(\tau)}{\varepsilon} \geq \frac{\log(\tau) - \gamma \log(M\omega)}{\log(1 - \varepsilon)}.$$

This implies that

$$\log(M\omega^\gamma(1 - \varepsilon)^n) \leq \log(\tau) \implies M\omega^\gamma(1 - \varepsilon)^n \leq \tau.$$

By the assumption that $\kappa(R) \leq M\omega^\gamma$ and the bound (3.2) on r , we find

$$\kappa(R)r^n \leq \tau.$$

Therefore, the last inequality in

$$\|\hat{e}_h^{(n)}\| \leq \kappa(R)r^n \|\hat{e}_h^{(0)}\| \leq \tau \|\hat{e}_h^{(0)}\|,$$

follows showing that the relation (3.6) holds. This concludes the proof of the theorem.

3.2. Supporting Lemmas. The proof of Theorem 3.1 relies Lemma 3.8 which is a corollary to Lemma 3.6. To prove Lemma 3.6 we additionally present Lemmas 3.4 and 3.5 (the proof of the latter can be found in [11]). The key observation is that the filter transfer function $\beta(\lambda)$ maps the left half of the complex plane to the unit disk, and that $|\beta(\lambda)| = 1$ only if $\lambda = \pm i\omega$. The parabolic bounds (3.1) are used to show a uniform bound on β .

LEMMA 3.4. *The scaled filter transfer function $\hat{\beta}$ is entire, and*

$$(3.15) \quad \hat{\beta}(z) = \begin{cases} -\frac{1}{2}, & z = 0, \\ 1, & z = \pm i, \\ \frac{3z^2 - 1}{4\pi z(z^2 + 1)} (e^{2\pi z} - 1), & \text{else.} \end{cases}$$

Proof. The expression (3.15) is given by a direct computation. The fact that $\hat{\beta}$ is entire can be demonstrated as follows. Define the piecewise continuous, bounded, and compactly supported function:

$$g(t) = \begin{cases} \cos(t) - \frac{1}{4}, & 0 \leq t \leq 2\pi, \\ 0, & \text{else.} \end{cases}$$

Note that

$$\pi\hat{\beta}(-z) = \int_0^{2\pi} \left(\cos(t) - \frac{1}{4} \right) e^{-zt} dt = \int_0^\infty g(t)e^{-zt} dt.$$

That is, $\pi\hat{\beta}(-z)$ is the Laplace transform of $g(t)$. It is a property of the Laplace transform [1] that because g is piecewise continuous, bounded, and compactly supported, $\pi\hat{\beta}(-z)$ is entire. Thus $\hat{\beta}$ is entire. \square

LEMMA 3.5. *For all $y \in \mathbb{R}$, the scaled filter transfer function $\hat{\beta}$ satisfies*

$$\begin{aligned} |\hat{\beta}(iy)| &\leq 1 - (y - 1)^2, & \text{when } |y - 1| \leq \frac{1}{2}, \\ |\hat{\beta}(iy)| &\leq 1 - (y + 1)^2, & \text{when } |y + 1| \leq \frac{1}{2}, \\ |\hat{\beta}(iy)| &\leq \frac{3}{4}, & \text{else.} \end{aligned}$$

This is a restatement of Lemma 2.1 in [3] and the proof may be found there.

LEMMA 3.6. *For all $\varepsilon > 0$ and for all $z = x + iy \in \mathbb{C}_-$, if*

$$(3.16) \quad -x + \alpha(y - 1)^2 \geq \varepsilon, \quad \text{and} \quad -x + \alpha(y + 1)^2 \geq \varepsilon,$$

where $\alpha = \frac{2\pi^2 - 3}{12\pi} \approx 0.44$ then

$$|\hat{\beta}(z)| \leq \max\{1 - \delta, 1 - \varepsilon\}.$$

Here $\delta < 1$ is a universal constant independent of ε .

Proof. In (3.15), observe that $\hat{\beta}$ is a rational function multiplied by $e^{2\pi z} - 1$. The denominator of the rational function is of higher order than the numerator, so this function tends to zero uniformly at infinity. Thus, since $e^{2\pi z} - 1$ is bounded for all $z \in \mathbb{C}_-$, $\hat{\beta}(z) \rightarrow 0$ uniformly as $|z| \rightarrow \infty$ for all $z \in \mathbb{C}_-$. Therefore, there exists a $R_0 \geq 2$ such that for all $z \in \mathbb{C}_-$ if $|z| \geq R_0$ then $|\hat{\beta}(z)| \leq \frac{3}{4}$.

Next we will bound $|\hat{\beta}|^2$ when $|z| \leq R_0$ and satisfying the parabolic bounds (3.16). Define the parabolic contours (see Figure 1):

$$C_\varepsilon = \{x + iy : -x + \alpha(y - 1)^2 = \varepsilon, x \leq 0\}, \quad C'_\varepsilon = \{x + iy : -x + \alpha(y + 1)^2 = \varepsilon, x \leq 0\}.$$

Define the regions:

$$\begin{aligned} G_\varepsilon &= \{x + iy : -x + \alpha(y - 1)^2 \leq \varepsilon, x \leq 0\}, \\ G'_\varepsilon &= \{x + iy : -x + \alpha(y + 1)^2 \leq \varepsilon, x \leq 0\}. \end{aligned}$$

Note that the boundary of G_ε is $\partial G_\varepsilon = C_\varepsilon \cup \{iy : (y + 1)^2 \leq \varepsilon/\alpha\}$. It is easy to verify that for any $0 < \varepsilon_1 \leq \varepsilon_2$ we have $G_{\varepsilon_1} \subseteq G_{\varepsilon_2}$, therefore $\mathbb{C}_- \setminus G_{\varepsilon_2} \subseteq \mathbb{C}_- \setminus G_{\varepsilon_1}$. We find a similar result for G'_ε in terms of C'_ε .

Next, define the compact region $D_\varepsilon \subset \mathbb{C}_-$ which is enclosed by C_ε , C'_ε , the imaginary axis, and the circle $|z| = R_0$ (see Figure 1). That is,

$$D_\varepsilon = \{z \in \mathbb{C}_- : |z| \leq R_0\} \setminus (G_\varepsilon \cup G'_\varepsilon).$$

We want to show that $|\hat{\beta}| \leq \max\{1 - \varepsilon, 1 - \delta\}$ (for some δ independent of ε) in D_ε for any $\varepsilon > 0$.

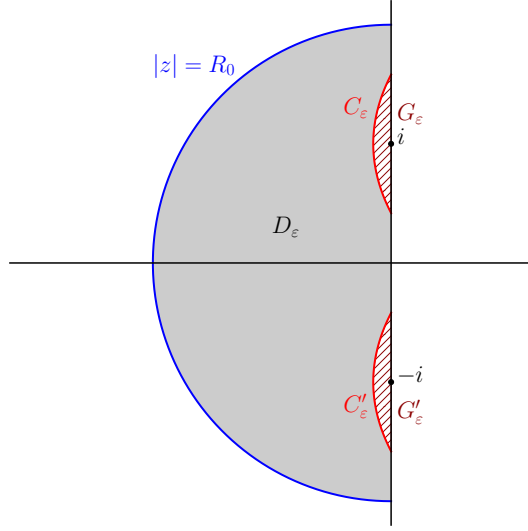


Fig. 1: The regions D_ε , G_ε , and G'_ε and contours C_ε and C'_ε for some small $\varepsilon < \frac{1}{2}$.

Because $\hat{\beta}$ is analytic (see Lemma 3.4), by the maximum modulus principle, the maximum value of $|\hat{\beta}|$ inside D_ε is attained on the boundary of D_ε , that is, either on the arc $|z| = R_0$, on C_ε , on C'_ε , or on the imaginary axis. By the choice of R_0 , $|\hat{\beta}| \leq \frac{3}{4}$ on the arc.

On the imaginary axis, if $z = iy \in \partial D_\varepsilon$, then $|y - 1| \geq \sqrt{\varepsilon/\alpha}$ and $|y + 1| \geq \sqrt{\varepsilon/\alpha}$ by the assumption of 3.16. Thus, from Lemma 3.5,

$$|\hat{\beta}(iy)| \leq \max \left\{ 1 - (y - 1)^2, 1 - (y + 1)^2, \frac{3}{4} \right\} \leq \max \left\{ 1 - \frac{\varepsilon}{\alpha}, \frac{3}{4} \right\}.$$

Next, consider the parabolic contour C_ε and the region G_ε . We first consider the case where $\sqrt{\varepsilon} \leq \min\{\sqrt{\alpha}, \frac{2\pi-2}{M_\alpha}\}$ where M_α depends only on α and will be defined shortly. This range of ε ensures that $\Im\{z\} \geq 0$ for every $z \in C_\varepsilon$ for every such ε . In Figure 1, this range of ε ensures C_ε and G_ε remain above the real axis. For every $z \in G_\varepsilon$ there is a $t \in [-1, 1]$ and $s \in [0, \sqrt{\varepsilon}]$ such that

$$z = z(s, t) := -s^2(1 - t^2) + i(1 + ts/\sqrt{\alpha}).$$

Note that $C_\varepsilon = \{z(\sqrt{\varepsilon}, t) : t \in [-1, 1]\}$, that is C_ε is parametrized by $z(s, t)$ with $s = \sqrt{\varepsilon}$ fixed. It can be checked that the power series of $|\hat{\beta}(z)|^2$ in s at $z = i$ is

$$|\hat{\beta}(z(s, t))|^2 = 1 - 2\pi s^2 + s^3 R(s, t).$$

Since $\hat{\beta}$ is analytic, then $|\hat{\beta}|^2$ is smooth, and $R(s, t)$ is continuous. Further, since G_ε is compact, there exists $M_\varepsilon < \infty$ such that

$$M_\varepsilon = \max_{z \in G_\varepsilon} |R(z(s, t))| = \max_{\substack{t \in [-1, 1] \\ s \in [0, \sqrt{\varepsilon}]}} |R(s, t)|.$$

Since $\sqrt{\varepsilon} \leq \sqrt{\alpha}$ then $G_\varepsilon \subseteq G_\alpha$, so $M_\alpha \geq M_\varepsilon$ (where M_α is similarly defined as the maximum of $|R|$ over G_α). Hence, since on C_ε , $s = \sqrt{\varepsilon}$, then for all $z \in C_\varepsilon$,

$$|\hat{\beta}(z)|^2 \leq 1 - 2\pi\varepsilon + M_\alpha\varepsilon^{3/2}.$$

Since we also assumed that $\sqrt{\varepsilon} \leq \frac{2\pi-2}{M_\alpha}$, then for all $z \in C_\varepsilon$

$$|\hat{\beta}(z)|^2 \leq 1 - 2\pi\varepsilon + M_\alpha\varepsilon \frac{2\pi-2}{M_\alpha} = 1 - 2\varepsilon.$$

To bound $|\hat{\beta}|^2$ on C'_ε , note that $\hat{\beta}$ restricted to the real numbers is real, so by the Schwarz Reflection Principle $\hat{\beta}(\bar{z}) = \hat{\beta}(z)$, thus $|\hat{\beta}(\bar{z})| = |\hat{\beta}(z)|$. Since $C'_\varepsilon = \{\bar{z} : z \in C_\varepsilon\}$, we have the same bound on C'_ε as for C_ε . Altogether for $\sqrt{\varepsilon} \leq \max\{\alpha, \frac{2\pi-2}{M_\alpha}\}$, if $z \in D_\varepsilon$, then (because $\frac{1}{\alpha} > 2$)

$$|\hat{\beta}(z)|^2 \leq \max \left\{ \left(\frac{3}{4} \right)^2, 1 - 2\varepsilon, \left(1 - \frac{\varepsilon}{\alpha} \right)^2 \right\} \leq \max \left\{ \left(\frac{3}{4} \right)^2, 1 - 2\varepsilon \right\}.$$

It remains to prove this result for $\sqrt{\varepsilon} > \min\{\sqrt{\alpha}, \frac{2\pi-2}{M_\alpha}\} =: \sqrt{\varepsilon_0}$. Note that on D_{ε_0} we have

$$|\hat{\beta}(z)|^2 \leq \max \left\{ \left(\frac{3}{4} \right)^2, 1 - 2\sqrt{\alpha}, 1 - 2\frac{2\pi-2}{M_\alpha} \right\} =: 1 - 2\delta.$$

Recall that by construction $\varepsilon > \varepsilon_0$ implies $\mathbb{C}_- \setminus G_\varepsilon \subset \mathbb{C}_- \setminus G_{\varepsilon_0}$ and thus $D_\varepsilon \subset D_{\varepsilon_0}$, so on D_ε

$$|\hat{\beta}(z)|^2 \leq 1 - 2\delta.$$

That is, for any $\varepsilon > 0$, inside D_ε we have $|\hat{\beta}(z)|^2 \leq \max\{1 - 2\varepsilon, 1 - 2\delta\}$. Therefore for all $z \in \mathbb{C}_-$ satisfying (3.16), we have

$$|\hat{\beta}(z)|^2 \leq \max\{1 - 2\delta, 1 - 2\varepsilon\}.$$

Finally, recall that for any $x \in [0, \frac{1}{2}]$, $\sqrt{1-2x} \leq 1-x$, so

$$|\hat{\beta}(z)| \leq \max\{1 - \delta, 1 - \varepsilon\}.$$

This proves the lemma. \square

Remark 3.7. A global optimization algorithm estimates $M_\alpha \approx 7.17$, so we can estimate

$$|\hat{\beta}(z)| \leq \max\left\{\frac{3}{4}, 1 - \varepsilon\right\}.$$

LEMMA 3.8. *Let S be the diagonal matrix with entries $S_{jj} = \beta(\lambda_j)$. If there exists an $\varepsilon > 0$ such that for all j , $\lambda_j/\omega = x + iy$ satisfy parabolic bounds (3.16), then*

$$\rho(S) \leq \max\{1 - \delta, 1 - \varepsilon\},$$

where $0 < \delta < 1$ is a universal constant given in Lemma 3.6.

Proof. Since all of the eigenvalues (scaled by $1/\omega$) satisfy (3.16), then by Lemma 3.6, for each j

$$|\beta(\lambda_j)| = |\hat{\beta}(\lambda_j/\omega)| \leq \max\{1 - \delta, 1 - \varepsilon\}.$$

Since S is a diagonal matrix with entries $S_{jj} = \beta(\lambda_j)$,

$$\rho(S) = \max_j |\beta(\lambda_j)| \leq \max\{1 - \delta, 1 - \varepsilon\},$$

which proves the Lemma. \square

4. Numerical Experiments. In this section, we will investigate the convergence of the WaveHoltz iteration for solving the Helmholtz equation

$$(4.1a) \quad \Delta \hat{u} + \omega^2 \hat{u} = f(x), \quad x \in \Omega,$$

$$(4.1b) \quad \mathbf{n} \cdot \nabla u = 0, \quad x \in \Gamma_N,$$

$$(4.1c) \quad i\omega u + \mathbf{n} \cdot \nabla u = 0, \quad x \in \Gamma_I.$$

Here Ω is a bounded open subset of \mathbb{R}^d for $d = 1$ or $d = 2$. The boundary of Ω is $\Gamma = \Gamma_N \cup \Gamma_I$ where Γ_N is a subset of the boundary with Neumann boundary conditions and Γ_I is a subset of the boundary with impedance boundary conditions which approximate the Sommerfeld radiation condition on the bounded domain. Since Γ_I approximates an open boundary, this boundary will correspond to an outflow condition for the wave equation in the WaveHoltz iteration. Some of the energy of the wave inside Ω will leak out of the domain over time at this boundary, so any convergent spatial discretization of the wave equation, which we write as the system of differential equations

$$(4.2) \quad \frac{d}{dt} w_h = Aw_h - F \cos(\omega t), \quad \text{or} \quad \frac{d}{dt} w_h = Aw_h - F \sin(\omega t),$$

should be dissipative, that is, all the eigenvalues of A must lie in \mathbb{C}_- .

We will consider two discretizations for the wave equation: the finite difference method (FD) and the discontinuous Galerkin method (DG). In the one dimensional experiments we will relate the eigenvalues and eigenvectors of the discretization matrix A to the convergence rate of WaveHoltz. Both the one dimensional and two dimensional test problems will exemplify case (A) in Section 3. We do not consider case (B) as it has already been studied in [3].

4.1. Numerical Methods.

4.1.1. Finite Difference Method. For the FD method we discretize the wave equation in first-order form:

$$u_t = v, \quad v_t = \Delta u - f(x) \cos(\omega t).$$

We apply the WaveHoltz iteration directly to this real-valued system, and recover the complex-valued estimate of the Helmholtz solution at iteration n with $\hat{u}_h \approx \hat{u}_h^{(n)} + \frac{1}{i\omega} \hat{v}_h^{(n)}$ (see Appendix B).

The boundary conditions for the wave equation that will correspond to Neumann and impedance are, respectively,

$$\begin{aligned} \mathbf{n} \cdot \nabla u &= 0, & x \in \Gamma_N, t > 0, \\ u_t + \mathbf{n} \cdot \nabla u &= v + \mathbf{n} \cdot \nabla u = 0, & x \in \Gamma_I, t > 0, \end{aligned}$$

where \mathbf{n} is the outward facing normal to the boundary.

In one dimension we discretize this problem in the computational domain $\Omega = (-1, 1)$. We approximate the spatial derivatives using central differences on the uniform grid $x_j = -1 + jh$, $j = 0, \dots, m$ (where $h = 2/m$) and introduce the grid functions $(u_j, v_j) \approx (u(x_j), v(x_j))$. Neumann conditions are approximated using ghost points and centered finite differences. For example at x_0 we would have $(u_1 - u_{-1})/2h = 0$. Outflow conditions are approximated similarly, using the ghost

nodes. For example at x_m we would have $v_m + (u_{m+1} - u_{m-1})/2h = 0$. The spatial discretization of the first order system is

$$\begin{aligned} \frac{d}{dt}u_j &= v_j, \\ \frac{d}{dt}v_j &= \frac{u_{j-1} - 2u_j + u_{j+1}}{h^2} - f(x_j) \cos(\omega t), \quad j = 0, \dots, m. \end{aligned}$$

This spatial discretization has error proportional to $h^2\omega^3$ for the Helmholtz problem, so, when we vary ω , we select h according to the rule $h^2\omega^3 = \text{const}$. Note that in (4.2) we write $w_h = (u_0, \dots, u_m, v_0, \dots, v_m)^T$ and $F = (0, \dots, 0, f(x_0), \dots, f(x_n))^T$.

In two dimensions the spatial discretization is similarly defined by applying the one dimensional derivative approximations in each direction of the two dimensional grid.

Our analysis on the convergence of w to the exact solution of the Helmholtz equation assumed that the system of differential equations in (4.2) is solved exactly in time, however we will solve this equation using a fourth order Runge-Kutta method of [6] with small Δt so that the temporal errors minimally affect the convergence rate. Throughout this section, $\|\cdot\|$ is the 2-norm.

4.1.2. Discontinuous Galerkin Method. For the DG method we discretize the wave equation in conservative form:

$$(4.3a) \quad p_t + \nabla \cdot \mathbf{u} = -\frac{1}{\omega} f(x) \sin(\omega t),$$

$$(4.3b) \quad \mathbf{u}_t + \nabla p = 0.$$

We use the nodal DG-FEM on a mesh of elements $I_j, j = 0, \dots, n$. On each element we compute the L^2 inner product against a test function φ ,

$$\begin{aligned} \int_{I_j} (p_h)_t \varphi \, dx - \int_{I_j} \mathbf{u}_h \cdot \nabla \varphi \, dx + \int_{\Gamma_j} (\mathbf{u}_h \cdot \mathbf{n})^\# \varphi \, ds &= -\frac{1}{\omega} \sin(\omega t) \int_{I_j} f \varphi \, dx, \\ \int_{I_j} (\mathbf{u}_h)_t \varphi \, dx - \int_{I_j} p_h \nabla \varphi \, dx + \int_{\Gamma_j} p_h^\# \varphi \, nds &= 0. \end{aligned}$$

Here $(\mathbf{u}_h \cdot \mathbf{n})^\#$ and $p_h^\#$ are numerical fluxes for the quantities $\mathbf{u} \cdot \mathbf{n}$ and p , respectively, on the element interface $\Gamma_j = \partial I_j$. We take these fluxes to be the central/average flux:

$$p_h^\# = \frac{1}{2}(p^- + p^+), \quad (\mathbf{u}_h \cdot \mathbf{n})^\# = \frac{1}{2}(\mathbf{u}^- + \mathbf{u}^+) \cdot \mathbf{n}.$$

We choose the sub-optimal central flux (rather than the upwind flux) because the upwind flux produces a matrix which is not diagonalizable. Hence, we cannot examine the assumptions of Theorem 3.1 in detail for this discretization. However, computational experiments in Section 4.3.2 show that the convergence results for both methods are very similar. The implementation is based on [18] and [17].

Here we can take p and \mathbf{u} to be real valued and recover the complex valued solution via the procedure in Appendix B.

4.2. Numerical Examples in One Dimension. Consider the problem:

$$(4.4a) \quad \frac{d^2 \hat{u}}{dx^2} + \omega^2 \hat{u} = f, \quad x \in (-1, 1),$$

$$(4.4b) \quad \frac{d\hat{u}}{dx}(-1) = 0, \quad i\omega \hat{u}(1) + \frac{d\hat{u}}{dx}(1) = 0.$$

In the following sections we will investigate the discretization matrices that arise from this problem via the finite difference and discontinuous Galerkin methods previously described. We will consider the eigenvalues and eigenvectors of these matrices for various values of ω and find that they satisfy the conditions of Theorem 3.1. We will then consider a test problem where we begin with a specially selected initial guess which has a slow rate of convergence at first, but eventually converges quickly.

4.2.1. Finite Difference. By Theorem 3.1, we expect WaveHoltz to converge with rate $r \leq 1 - \varepsilon$ where ε depends on distance between the eigenvalues of the discretization matrix A and $i\omega$. We verify this convergence rate for ω between 10π and 30π . We choose $h^2\omega^3 = 10$ which will correspond to approximately 10 points per wavelength for $\omega = 10\pi$. First we plot the eigenvalues of A scaled by $1/\omega$ for $\omega = 10\pi, 20\pi$, and 30π in Figure 2. As ω increases, the scaled eigenvalues get closer to the imaginary axis. Note that the imaginary part is much larger in magnitude than the real part. The black contours are level sets of the parabolic distance in Theorem 3.1. Observe that the parabolic distance is more sensitive to changes in the real direction than the imaginary direction. For each ω , all the eigenvalues are well separated from $i\omega$ and the parabolic distance ε^* appears to decrease as $1/\omega$. The distance $|\lambda^* - i\omega|$ then only depends weakly on ω , so we predict that WaveHoltz will converge in $N \sim O(\omega)$ iterations, based on the discussion in Section 3, case (A).

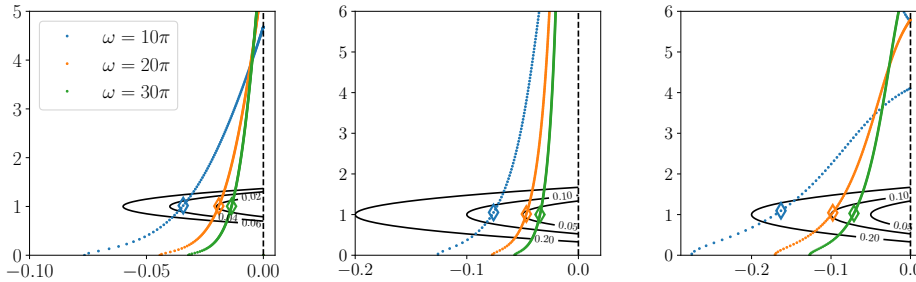


Fig. 2: The eigenvalues of the discretization matrix A scaled by $1/\omega$ for finite differences (left) and DG with $P = 1$ (middle) and $P = 2$ (right). Because A is real, all of its eigenvalues are either real or appear in complex conjugate pairs, so we plot the eigenvalues where $\Im\{\lambda\} \geq 0$. The diamonds are λ^*/ω as in (3.8), the eigenvalues closest to $i\omega$ in the sense of the parabolic distance of which we draw three level sets. As ω increases we observe the distance between $i\omega$ and the nearest eigenvalue decreasing.

In Figure 3 we plot ε^* (the minimum parabolic distance of the eigenvalues from $i\omega$ as in (3.9)) and $1 - \rho(\mathcal{S}_h)$ for various ω . Note by Lemma 3.8, $\varepsilon^* \leq 1 - \rho(\mathcal{S}_h)$. For this discretization we see that ε^* decreases sublinearly in terms of ω which suggests that WaveHoltz should converge quickly for this problem. We also plot the condition number $\kappa(m(\omega))$ introduced in Theorem 3.1. The assumption that κ is bounded by a power of ω is also verified for this range of ω , and it appears that $\kappa(m(\omega)) \sim O(\omega^3)$.

Next, we examine the convergence for a particular choice of right-hand-side, f . Following the reasoning in Section 2.2, we will study the convergence rate by exam-

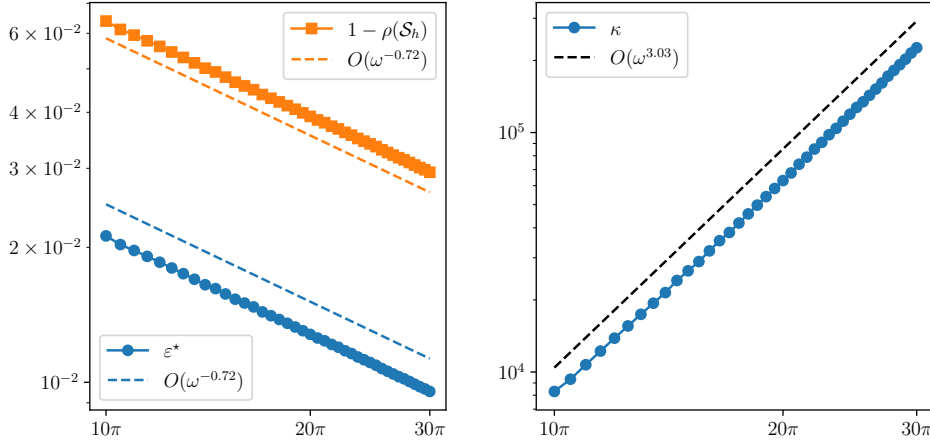


Fig. 3: (left) Optimal ε^* vs. ω (left). Condition number $\kappa(m)$ vs. ω (right). The slopes of the dashed lines for both plots were estimated by regression.

ining the error $\hat{e}_h^{(n)} = \hat{w}_h^{(n)} - \hat{w}_h^*$ which is given by the fixed point iteration:

$$\hat{e}_h^{(n+1)} = \mathcal{S}_h \hat{e}_h^{(n)} = \mathcal{S}_h^{n+1} \hat{e}_h^{(0)}.$$

We also consider the norm of the error in the coefficients of the eigenvectors $\mu_h^{(n)}$ which are defined as

$$\mu_h^{(n)} := R^{-1} \hat{e}_h^{(n)}.$$

As suggested in by Theorem 3.1 we expect the WaveHoltz iteration to converge with rate proportional to $1 - \varepsilon^*$. Since in Figure 3 we observed that $\varepsilon^* \sim O(\omega^{-0.72})$, hence for this problem we expect

$$\frac{\|\mu_h^{(n+1)}\|}{\|\mu_h^{(n)}\|} \sim O(1 - \omega^{-0.72}),$$

and, since $\kappa \sim O(\omega^{3.01})$, we also expect

$$\frac{\|\hat{e}_h^{(n)}\|}{\|\hat{e}_h^{(0)}\|} \sim O(\omega^{3.01}(1 - \omega^{-0.72})^n).$$

We chose $\hat{e}_h^{(0)}$ as,

$$(4.5) \quad \begin{aligned} u_0(x) &= 2 \sin^2(\pi x) \sin(\omega x), \\ \hat{e}_h^{(0)} &= (u_0, -\frac{d}{dx} u_0). \end{aligned}$$

Here, the right-hand-side, f , is implicitly defined in terms of the initial error. With our choice of initial condition, we observe an initial convergence rate of

$$\frac{\|\hat{e}_h^{(1)}\|}{\|\hat{e}_h^{(0)}\|} \sim O(1 - \omega^{-2}),$$

which is substantially slower than the estimated rate for μ_h . Define the average converge rate as

$$\bar{r}_e = \frac{1}{K} \sum_{k=0}^{K-1} \frac{\|\hat{e}_h^{(k+1)}\|}{\|\hat{e}_h^{(k)}\|}.$$

In Figure 4, we show the convergence rate for the first iteration and compare it to the rate averaged over $K = 1000$ iterations. While the first iteration is slow in \hat{e}_h , the convergence rate for μ_h is better than estimated by the $1 - \varepsilon^*$ bound. As we take more iterations we observe $\bar{r}_e \approx \bar{r}_\mu \sim O(1 - \omega^{-0.71})$ which matches the expected rate from the model for $1 - \varepsilon^*$. In Figure 5 we plot the relative error for the first one thousand iterations for selected values of ω . We see that the true error $\|\hat{e}_h\|$ may sometimes stagnate or even briefly increases, but may also decrease much faster than $\|\mu_h\|$. As already seen in Figure 4, the average convergence rate for $\|\hat{e}_h\|$ almost exactly matches the rate for $\|\mu_h\|$.

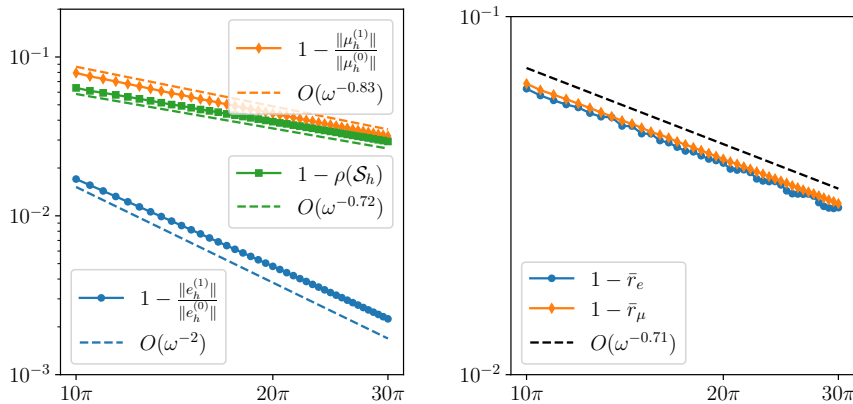


Fig. 4: One minus the convergence rate for the first iteration as a function of ω (left). One minus the convergence rate averaged over one thousand iterations (right).

4.2.2. Discontinuous Galerkin. Consider the Helmholtz equation in (4.4). We discretize this problem with uniformly spaced elements and degrees of freedom specified on the Legendre-Gauss-Lobatto quadrature points. The order of the DG discretization is $P + \frac{1}{2}$ where P is the degree of the polynomial basis functions on each element. Like in the finite difference discretization we choose our degrees of freedom according to $h^{P+\frac{1}{2}}\omega^{P+\frac{3}{2}} = 10$.

In Figure 2 we plot the eigenvalues for discretizations of all combinations of $P = 1, 2$ and $\omega = 10\pi, 20\pi, 30\pi$. As with the finite difference case, the eigenvalues are bounded away from $i\omega$, and since the real part of this distance is relatively large, we should expect fast convergence. Note that this distance is roughly two orders of magnitude larger than for the finite difference case. This difference is reflected in the convergence rates of these methods as DG converges much faster for this problem than FD. We postulate that this is a consequence of the accuracy of the impedance boundary conditions. In one dimension, the DG scheme's non-reflecting boundary conditions are exact to machine precision, whereas the finite difference boundary condition is $O(h^2)$, so it takes longer to dissipate the non-time-harmonic waves.

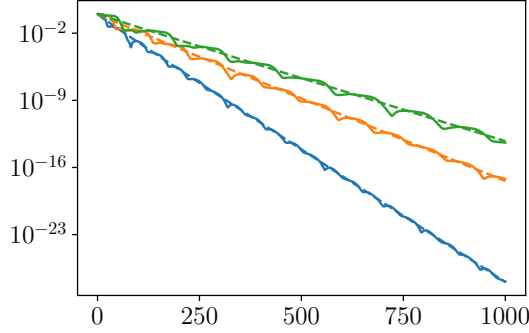


Fig. 5: Relative error for the first one thousand iterations for $\omega = 10\pi, 20\pi, 30\pi$ (blue, orange, green). The solid lines are $\frac{\|\hat{e}_h^{(k+1)}\|}{\|\hat{e}_h^{(k)}\|}$ and the dashed lines $\frac{\|\hat{\mu}_h^{(k+1)}\|}{\|\hat{\mu}_h^{(k)}\|}$.

In Figure 6 we plot one minus the estimated convergence rate $1 - \varepsilon^*$ and $\rho(\mathcal{S}_h)$ for uniformly spaced values of ω . Additionally, we plot the condition number of the eigenvector matrix. We see that the precise convergence rate $\rho(\mathcal{S}_h)$ is slightly better than the estimate and gets closer to 1 sublinearly for both $P = 1$ and $P = 2$ as ω increases. The condition number κ appears to be polynomially bounded for both $P = 1$ and $P = 2$. Despite a fairly high polynomial power for $P = 2$, the convergence is much faster than for the finite difference case as seen in Figure 7.

As for the finite difference example, we examine the convergence rate in terms of \hat{e}_h and μ_h for the initial condition (4.5). In Figure 7 we plot the convergence rate of the first iteration. For each P , the convergence rate of μ_h is sublinear but the convergence rate of \hat{e}_h is approximately $O(1 - \omega^{-2})$. As before, we plot the convergence rate averaged over the first one thousand iterations, \bar{r} . We find that $\bar{r}_e \approx \bar{r}_\mu \sim O(1 - \omega^{-0.75})$ and is slightly better for $P = 1$ than $P = 2$.

4.3. Numerical Experiments in Two Dimensions. We now consider the Helmholtz equation (4.1) in two dimensions on the domain $\Omega = (-1, 1) \times (-1, 1)$. We use Neumann boundary conditions at $x = -1$ and $y = -1$ and outflow boundary conditions at $x = 1$ and $y = 1$. We place a "point"-source forcing term centered at $(-0.7, -0.1)$ which depends on the frequency ω

$$f(x, y) = \pi^{-1} \omega^2 e^{-\omega^2[(x+0.7)^2 + (y+0.1)^2]}.$$

Due to the number of degrees of freedom needed to resolve the solution, computing the eigenvalues and eigenvectors is computationally very difficult for even moderate frequencies ω . Instead, we will examine the iteration directly. We start by analyzing the convergence behaviour by looking at the relative residual of the iteration:

$$\text{res}^{(n)} = \frac{\|\hat{w}_h^{(n)} - \hat{w}_h^{(n-1)}\|}{\|\hat{w}_h^{(1)} - \hat{w}_h^{(0)}\|} = \frac{\|\hat{w}_h^{(n-1)} - \Pi_h \hat{w}_h^{(n-1)}\|}{\|\hat{w}_h^{(0)} - \Pi_h \hat{w}_h^{(0)}\|}.$$

The residual is an estimate of the relative error $\text{res}^{(n)} \approx \frac{\|\hat{e}_h^{(n)}\|}{\|\hat{e}_h^{(0)}\|}$ but is a more practical metric since we do not assume we have access to \hat{w}_h^* during the iteration. We will

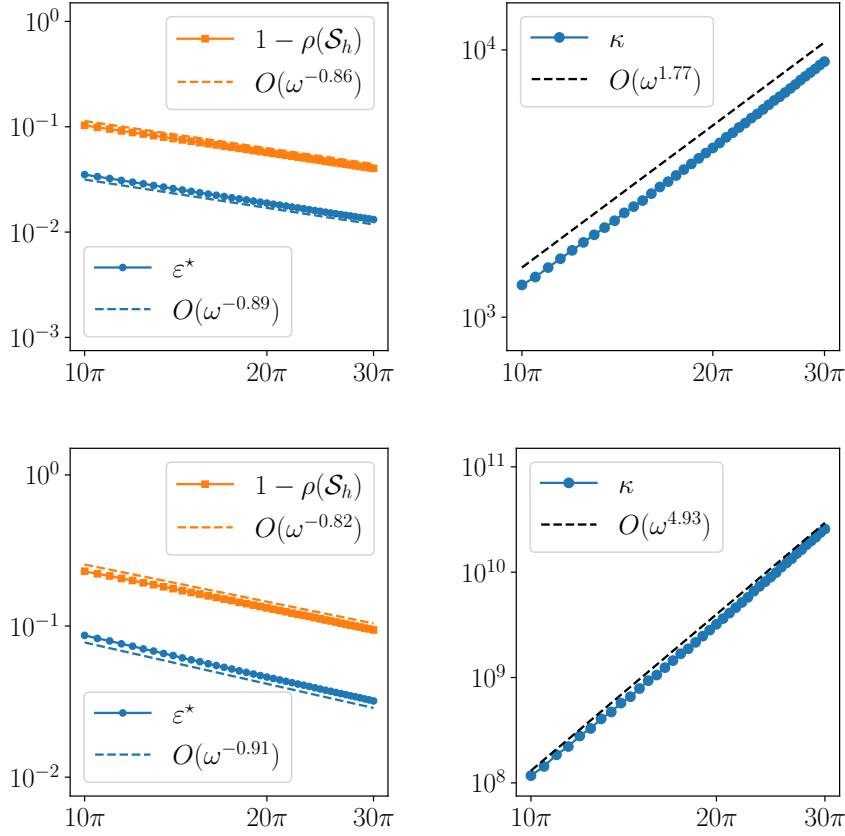


Fig. 6: Optimal ε^* vs. ω (left). Condition number $\kappa(m)$ vs. ω (right). The slopes of the dashed lines for both plots were estimated by regression. The top pair of plots correspond to $P = 1$, and the bottom pair correspond to $P = 2$.

also model the number of iterations $N(\tau, \omega)$ needed to reach a specified tolerance. For these examples, we specify a tolerance of $\tau = 10^{-6}$.

4.3.1. Finite Difference. In Figure 8 we plot the relative residual as a function of the number of iterations for the first one thousand iterations for $\omega = 10\pi, 20\pi$, and 30π . We see that for all three frequencies, the number of iterations drops readily, and well below the desired tolerance within the first one thousand iterations. Of note is the relative residual for $\omega = 10\pi$ which appears to reach machine precision at around 700 iterations. In Figure 9 we plot the number of iterations to reach the specified relative residual of 10^{-6} for uniformly spaced frequencies. The number of iterations $N \sim O(\omega^{0.79})$ in this range of frequencies which is consistent with the one dimensional test problem.

4.3.2. Discontinuous Galerkin. We repeat the experiment from the finite difference example using the discontinuous Galerkin method. In addition to the central

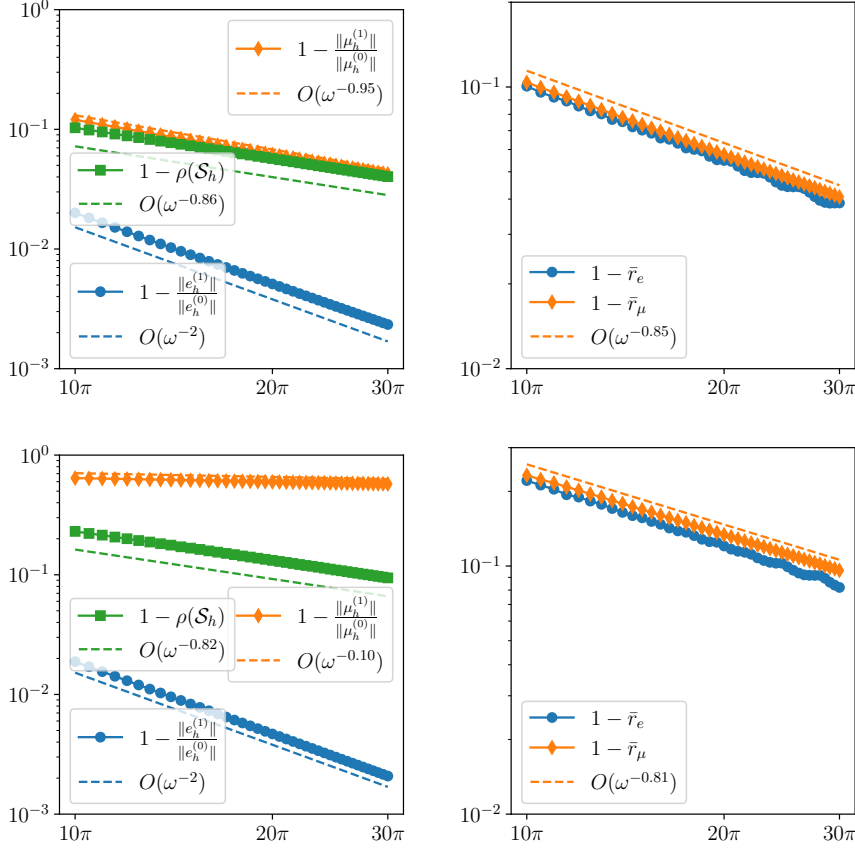


Fig. 7: One minus the convergence rate for the first iteration as a function of ω (left). One minus the convergence rate averaged over one thousand iterations (right). The upper pair correspond to $P = 1$, and the lower pair correspond to $P = 2$.

flux, we will also consider the upwind flux

$$p_h^\# = \frac{1}{2}(p^- + p^+) + \frac{1}{2}\mathbf{n} \cdot (\mathbf{u}^- - \mathbf{u}^+), \quad \mathbf{u}_h^\# = \frac{1}{2}\mathbf{n} \cdot (\mathbf{u}^+ + \mathbf{u}^-) + \frac{1}{2}(p^- - p^+).$$

The DG scheme with upwind flux is not diagonalizable, and therefore there is less we can specifically say about its convergence behaviour. Nevertheless, we will see that the upwind scheme converges just as quickly as the DG scheme with the central flux. In Figure 8 we plot the relative residual as a function of the number of iterations for the first one thousand iterations for $\omega = 10\pi, 20\pi$, and 30π . Like in the one dimensional case, the DG method converges much faster than the finite difference, with both $\omega = 10\pi$ and $\omega = 20\pi$ reaching machine tolerance within the first one thousand iterations. It is interesting that for the central flux, both $P = 1$ and $P = 2$ produced near identical relative residuals throughout the iteration. If the convergence rate is independent of the order, then it may prove more efficient and more accurate to apply WaveHoltz iteration to higher order methods because we can take h to be larger (especially for high frequency). However, we do not investigate this further here. For

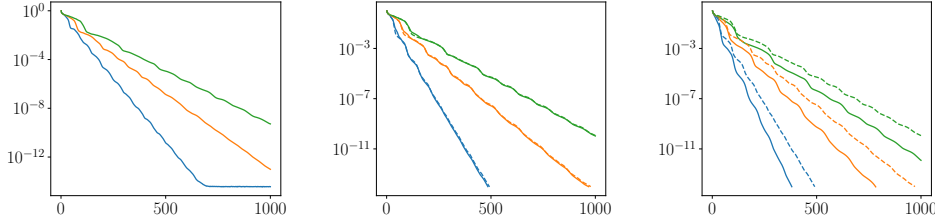


Fig. 8: The relative residual $\text{res}^{(n)}$ for $\omega = 10\pi, 20\pi, 30\pi$ (blue, orange, green) vs. the number of iterations for the first 1000 iterations using the finite difference method (left) the DG scheme with central (middle) and upwind (right) fluxes. Upwind DG with $P = 1$ (solid) converges faster than for $P = 2$ (dashed).

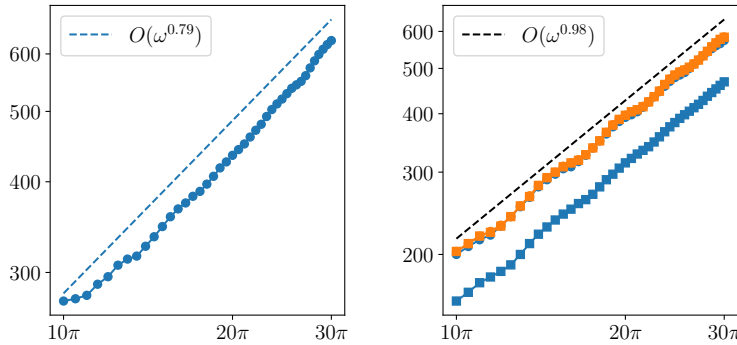


Fig. 9: The number of iterations needed to reach a tolerance of 10^{-6} for ω in the range of 10π to 30π . To the left are results obtained by the finite difference discretization and to the right the results from the DG discretization ($P = 1$ in blue, $P = 2$ in orange, upwind are squares, central are circles). Note that with $P = 1$ and upwind flux, WaveHoltz converges much faster than with upwind $P = 2$ or the central flux scheme with $P = 1$ or $P = 2$.

the upwind scheme, however, we observe that the lower order $P = 1$ converges faster than $P = 2$. This difference is likely because the upwind scheme is fairly dissipative (more so for lower order) which further shifts the real part of the eigenvalues away from the real axis, and therefore allows faster convergence of the WaveHoltz iteration.

In Figure 9 we plot the number of iterations to reach the specified relative residual of 10^{-6} for uniformly spaced frequencies in the range 10π to 30π . As suggested by Figure 8, the DG methods with $P = 1$ and $P = 2$ display a near identical relationship between the frequency and the number of iterations. It seems that for these two low order DG schemes, the number of iterations $N \sim O(\omega)$ in this range of frequencies.

5. Conclusions. We generalized previous results on the convergence of the WaveHoltz iteration to problems obtained by applying the WaveHoltz algorithm to the wave equation discretized in space. We proved that this semi-discrete WaveHoltz algorithm converges to an approximate solution of the Helmholtz equation for any sta-

ble discretization (regardless of boundary conditions). We estimated the convergence rate of the iteration as the (parabolic) distance of the eigenvalues of the spatial discretization matrix from $\pm i\omega$. This estimate was found to be modest compared to the true convergence rate for the numerical examples considered. We believe that tighter bounds on the convergence rate are possible, but this analysis is left to the future. We presented numerical examples verifying the assumptions of the main theorem. An immediate future extension of the results here are to consider the convergence rate of the WaveHoltz iteration when accelerated with Krylov space methods.

Appendix A. Proof of Theorem 3.2. The proof of Theorem 3.2 proceeds in much the same way as the proof of Theorem 3.1, but relies on different results from linear algebra and the following two lemmas:

LEMMA A.1 (Greenbaum [14] Theorem 1.3.3). *Let A be an $n \times n$ complex or real matrix and let $\epsilon > 0$. There is a norm $\|\cdot\|_{A,\epsilon}$ on \mathbb{C}^m whose induced matrix norm satisfies*

$$\rho(A) \leq \|A\|_{A,\epsilon} \leq \rho(A) + \epsilon.$$

LEMMA A.2. *We can express β as the power series*

$$\beta(z) = \sum_{n=0}^{\infty} b_n z^n.$$

Here

$$b_n = \frac{2}{T} \int_0^T \left(\cos(\omega t) - \frac{1}{4} \right) \frac{t^n}{n!} dt.$$

Proof. We simply substitute the power series for e^{tz} into the integral definition of $\beta(z)$ and swap the order of the sum and the integral. Since the domain is bounded and the integrands are continuous, then each b_n is finite, moreover, $|b_n| \leq \frac{1}{n!}$, so swapping the sum and integral is justified (by Fubini's theorem). \square

The proof of Theorem 3.2 is as follows.

Proof. As with Theorem 3.1 we examine the residual $\hat{e}_h^{(n)} := \hat{w}_h^{(n)} - \hat{w}_h^*$. Recall,

$$(A.1) \quad \hat{e}_h^{(n)} = (\mathcal{S}_h)^n \hat{e}_h^{(0)}.$$

If $\hat{e}_h^{(n)} \rightarrow 0$, then $\hat{w}_h^{(n)} \rightarrow \hat{w}_h^*$, so we must show that \mathcal{S}_h is eventually contractive, that is, there is some power k , such that $\|(\mathcal{S}_h)^k\| < 1$. To this end, it is sufficient to show that $\rho(\mathcal{S}_h) < 1$ which we achieve by relating \mathcal{S}_h to A .

The product $\mathcal{S}_h \hat{e}_h$ is

$$(A.2a) \quad \mathcal{S}_h \hat{e}_h = \frac{2}{T} \int_0^T \left(\cos(\omega t) - \frac{1}{4} \right) e_h(t) dt,$$

$$(A.2b) \quad \frac{de_h}{dt} = A e_h,$$

$$(A.2c) \quad e_h(0) = \hat{e}_h.$$

Let $A = RJR^{-1}$ be the Jordan normal form of A , then the solution to (A.2b) is

$$e_h(t) = e^{tA} \hat{e}_h = R e^{tJ} R^{-1} \hat{e}_h.$$

and thus,

$$\mathcal{S}_h \hat{e}_h = R \left(\frac{2}{T} \int_0^T \left(\cos(\omega t) - \frac{1}{4} \right) e^{tJ} dt \right) R^{-1} \hat{e}_h.$$

Substitute the power series representation of the matrix exponential and swap the order of the integral like in Lemma A.2 to find,

$$\mathcal{S}_h \hat{e}_h = R \left(\sum_{n=0}^{\infty} b_n J^n \right) R^{-1} \hat{e}_h$$

Since this is true for any \hat{e}_h , we conclude that

$$(A.3) \quad \mathcal{S}_h = R \left(\sum_{n=0}^{\infty} b_n J^n \right) R^{-1} =: RSR^{-1}.$$

Let J_k be the $k \times k$ Jordan block corresponding to eigenvalue λ . Then, via the power series of β in Lemma A.2, it can be verified that S will have the same block structure as J and the block S_k corresponding to J_k is

$$S_k = \begin{pmatrix} \beta(\lambda) & \beta'(\lambda) & \frac{1}{2}\beta''(\lambda) & \cdots & \frac{1}{(k-1)!}\beta^{(k-1)}(\lambda) \\ 0 & \beta(\lambda) & \beta'(\lambda) & \vdots & \frac{1}{(k-2)!}\beta^{(k-2)}(\lambda) \\ 0 & 0 & \ddots & \ddots & \vdots \\ \vdots & \cdots & \ddots & \beta(\lambda) & \beta'(\lambda) \\ 0 & \cdots & \cdots & 0 & \beta(\lambda) \end{pmatrix}$$

Note that S is upper triangular, and therefore, its eigenvalues are the eigenvalues of A mapped by the filter-transfer function β . By assumption there exists an $\varepsilon > 0$ such that for each j ,

$$-\Re\{\lambda_j/\omega\} + \alpha(\Im\{\lambda_j/\omega\} - 1)^2 \geq \varepsilon, \quad \text{and} \quad -\Re\{\lambda_j/\omega\} + \alpha(\Im\{\lambda_j/\omega\} + 1)^2 \geq \varepsilon.$$

Thus by Lemma 3.8,

$$\beta(\lambda_j) \leq \max\{1 - \varepsilon, 1 - \delta\} < 1.$$

Since the eigenvalues of S are $\beta(\lambda_j)$ and since \mathcal{S}_h and S are similar (by (A.3)) we have that

$$\rho(S) = \rho(\mathcal{S}_h) \leq \max\{1 - \varepsilon, 1 - \delta\}.$$

Let $\|\cdot\|_{\mathcal{S}_h, \varepsilon}$ be the norm in Lemma A.1 for \mathcal{S}_h and pick $\varepsilon = \frac{1}{2} \min\{\varepsilon, \delta\}$. Then substituting (A.3) into (A.1) we have,

$$(A.4) \quad \hat{e}_h^{(n)} = R S^n R^{-1} \hat{e}_h^{(0)}.$$

Computing the $\|\cdot\|_{\mathcal{S}_h, \varepsilon}$ norm of both sides and using the sub-multiplicative property of the matrix norm we conclude that

$$\|\hat{e}_h^{(n)}\|_{\mathcal{S}_h, \varepsilon} \leq r^n \cdot \|\hat{e}_h^{(0)}\|_{\mathcal{S}_h, \varepsilon},$$

where $r = \rho(S) + \varepsilon \leq \max\{1 - \frac{1}{2}\delta, 1 - \frac{1}{2}\varepsilon\}$. Using the equivalence of norms in finite dimensional spaces, there is a constant K which depends on A (and therefore ε) and the norm $\|\cdot\|$ such that

$$\|\hat{e}_h^{(n)}\| \leq K r^n \cdot \|\hat{e}_h^{(0)}\|.$$

Thus demonstrating (3.11). \square

Appendix B. WaveHoltz with Real Valued Wave Equation. Consider the real valued wave equation in conservative form

$$(B.1a) \quad p_t + \nabla \cdot \mathbf{u} = -\frac{1}{\omega} f(x) \sin(\omega t), \quad \mathbf{u}_t + \nabla p = 0.$$

The corresponding complex valued Helmholtz equation is

$$(B.2a) \quad i\omega \hat{p} + \nabla \cdot \hat{\mathbf{u}} = -\frac{1}{i\omega} f(x), \quad i\omega \hat{\mathbf{u}} + \nabla \hat{p} = 0.$$

When eliminating $\hat{\mathbf{u}}$ we find

$$\Delta \hat{p} + \omega^2 \hat{p} = f.$$

Which is the target Helmholtz equation. Taking the real and imaginary parts of equation B.2 results in the equations

$$\begin{aligned} -\omega \Im\{\hat{p}\} + \Re\{\nabla \cdot \hat{\mathbf{u}}\} &= 0, & \omega \Re\{\hat{p}\} + \Im\{\nabla \cdot \hat{\mathbf{u}}\} &= \frac{1}{\omega} f, \\ -\omega \Im\{\hat{\mathbf{u}}\} + \Re\{\nabla \hat{p}\} &= 0, & \omega \Re\{\hat{\mathbf{u}}\} + \Im\{\nabla \hat{p}\} &= 0. \end{aligned}$$

If we look for solutions to wave equation (4.3) of the form

$$\begin{aligned} p &= p_0 \cos(\omega t) - p_1 \sin(\omega t), \\ \mathbf{u} &= \mathbf{u}_0 \cos(\omega t) - \mathbf{u}_1 \sin(\omega t), \end{aligned}$$

then,

$$\begin{aligned} -\omega p_0 \sin(\omega t) - \omega p_1 \cos(\omega t) + \nabla \cdot \mathbf{u}_0 \cos(\omega t) - \nabla \cdot \mathbf{u}_1 \sin(\omega t) &= \frac{1}{\omega} f \sin(\omega t) \\ -\omega \mathbf{u}_0 \sin(\omega t) - \omega \mathbf{u}_1 \cos(\omega t) + \nabla p_0 \cos(\omega t) - \nabla p_1 \sin(\omega t) &= 0. \end{aligned}$$

By matching the cosine and sine terms, we find that

$$\begin{aligned} -\omega p_1 + \nabla \cdot \mathbf{u}_0 &= 0, & \omega p_0 + \nabla \cdot \mathbf{u}_1 &= \frac{1}{\omega} f, \\ -\omega \mathbf{u}_1 + \nabla p_0 &= 0, & \omega \mathbf{u}_0 + \nabla p_1 &= 0. \end{aligned}$$

These equations are the same as those for the real and imaginary parts of \hat{p} and $\hat{\mathbf{u}}$, so we can conclude

$$\hat{p} = p_0 + ip_1 \quad \hat{\mathbf{u}} = \mathbf{u}_0 + i\mathbf{u}_1.$$

Moreover, we use the equations above to find

$$p_1 = \frac{1}{\omega} \nabla \cdot \mathbf{u}_0,$$

Noting that $p(0, x) = p_0$ and $\mathbf{u}(0, x) = \mathbf{u}_0$, we find that (p_0, \mathbf{u}_0) is a fixed point of $(p, \mathbf{u}) = \Pi(p, \mathbf{u})$ so we can simply apply the WaveHoltz iteration with real function p and \mathbf{u} using the time domain equations (4.3), and extract the Helmholtz solution as

$$\hat{p} = p - \frac{1}{i\omega} \nabla \cdot \mathbf{u}.$$

- [1] M. ABRAMOWITZ AND I. A. STEGUN, *Handbook of mathematical functions with formulas, graphs, and mathematical tables*, U.S. Govt. Print. Off., 1964.
- [2] D. APPELÖ, F. GARCIA, A. A. LOYA, AND O. RUNBORG, *El-WaveHoltz: A time-domain iterative solver for time-harmonic elastic waves*, *Computer Methods in Applied Mechanics and Engineering*, 401 (2022), p. 115603.
- [3] D. APPELÖ, F. GARCIA, AND O. RUNBORG, *Waveholtz: Iterative solution of the Helmholtz equation via the wave equation*, *SIAM journal on scientific computing*, 42 (2020), pp. A1950–A1983.
- [4] A. BRANDT AND I. LIVSHITS, *Wave-ray multigrid method for standing wave equations*, *Electronic Transactions on Numerical Analysis*, (1997), pp. 162–181.
- [5] M. BRISTEAU, R. GLOWINSKI, AND J. PÉRIAUX, *Controllability methods for the computation of time-periodic solutions; application to scattering*, *Journal of Computational Physics*, 147 (1998), pp. 265–292.
- [6] M. H. CARPENTER AND C. A. KENNEDY, *Fourth-order 2N-storage Runge-Kutta schemes*, tech. rep., NASA, 1994.
- [7] B. DEPRÉS, *Méthodes de décomposition de domaines pour les problèmes de propagation d’ondes en régime harmonique*, PhD thesis, (1991).
- [8] B. ENGQUIST AND L. YING, *Sweeping preconditioner for the Helmholtz equation: Hierarchical matrix representation*, *Communications on pure and applied mathematics*, 64 (2011), pp. 697–735.
- [9] Y. A. ERLANGGA, *Advances in iterative methods and preconditioners for the Helmholtz equation*, *Archives of computational methods in engineering*, 15 (2008), pp. 37–66.
- [10] O. G. ERNST AND M. J. GANDER, *Why it is difficult to solve Helmholtz problems with classical iterative methods*, in *Numerical Analysis of Multiscale Problems, Lecture Notes in Computational Science and Engineering*, Springer Berlin Heidelberg, Berlin, Heidelberg, 2011, pp. 325–363.
- [11] F. GARCIA, D. APPELÖ, AND O. RUNBORG, *Extensions and analysis of an iterative solution of the Helmholtz equation via the wave equation*, arXiv preprint arXiv:2205.12349, (2022).
- [12] A. GILLMAN, A. BARNETT, AND P.-G. MARTINSSON, *A spectrally accurate direct solution technique for frequency-domain scattering problems with variable media*, *BIT Numerical Mathematics*, 55 (2015), pp. 141–170.
- [13] R. GLOWINSKI AND T. ROSSI, *A mixed formulation and exact controllability approach for the computation of the periodic solutions of the scalar wave equation. (i): Controllability problem formulation and related iterative solution*, *Comptes Rendus Math.*, 343 (2006), pp. 493–498.
- [14] A. GREENBAUM, *Iterative Methods for Solving Linear Systems*, Society for Industrial and Applied Mathematics, 1997.
- [15] M. GROTE AND J. TANG, *On controllability methods for the Helmholtz equation*, *Journal of Computational and Applied Mathematics*, 358 (2019), pp. 306–326.
- [16] M. J. GROTE, F. NATAF, J. H. TANG, AND P.-H. TOURNIER, *Parallel controllability methods for the Helmholtz equation*, *Computer Methods in Applied Mechanics and Engineering*, 362 (2020), p. 112846.
- [17] J. S. HESTHAVEN AND T. WARBURTON, *Nodal Discontinuous Galerkin Methods Algorithms, Analysis, and Applications*, Texts in Applied Mathematics, Springer New York, New York, NY, 1st ed. 2008. ed., 2008.
- [18] D. A. KOPRIVA, *Implementing Spectral Methods for Partial Differential Equations: Algorithms for Scientists and Engineers*, Scientific Computation, Springer Netherlands, 2009.
- [19] Y. J. LIU, S. MUKHERJEE, N. NISHIMURA, M. SCHANZ, W. YE, A. SUTRADHAR, E. PAN, N. A. DUMONT, A. FRANGI, AND A. SAEZ, *Recent Advances and Emerging Applications of the Boundary Element Method*, *Applied Mechanics Reviews*, 64 (2012), p. 030802.
- [20] Z. PENG AND D. APPELÖ, *EM-WaveHoltz: A flexible frequency-domain method built from time-domain solvers*, *IEEE Transactions on Antennas and Propagation*, 70 (2022), pp. 5659–5671.
- [21] C. C. STOLK, *A time-domain preconditioner for the Helmholtz equation*, *SIAM Journal on Scientific Computing*, 43 (2021), pp. A3469–A3502.
- [22] S. WANG, M. DE HOOP, AND J. XIA, *On 3d modeling of seismic wave propagation via a structured parallel multifrontal direct Helmholtz solver*, *Geophysical Prospecting*, 59 (2011), pp. 857–873.